TEST RESULTS FOR ROTORDYNAMIC COEFFICIENTS OF THE SSME HPOTP TURBINE INTERSTAGE SEAL WITH TWO SWIRL BRAKES*

Dara W. Childs, Erian Baskharone, and Christopher Ramsey
Turbomachinery Laboratory
Mechanical Engineering Department
Texas A&M University
College Station, Texas 77843-3123, U.S.A.

Test results are presented for the HPOTP Turbine Interstage Seal with both the current and an alternate, aerodynamically-designed, swirl brake. Tests were conducted at speeds out to 16,000 *rpm*, supply pressures up to 18.3 *bars*, and the following three inlet-tangential-velocity conditions: (a) no preswirl, (b) intermediate preswirl in the direction of rotation, and (c) high preswirl in the direction of rotation. The back pressure can be controlled independently and was varied to yield the following four pressure ratios: 0.4, 0.45, 0.56, and 0.67.

The central and simplest conclusion to be obtained from the test series is that the alternate swirl brake consistently outperforms the current swirl brake in terms of stability performance. The alternate swirl-brake's whirl-frequency ratio was generally about one half or less than corresponding values for the current design. In many cases, the alternate design yielded negative whirl-frequency-ratio values in comparison to positive values for the current design. The alternate design can be directly substituted into the space currently occupied by the current design. There is no change in leakage performance.

*The work reported herein was supported by NASA Lewis Research Center under contract NAG3-181; contract technical monitor: Robert Hendricks.

NOMENCLATURE

A	Rotor shake amplitude (L)
C, c	Direct and cross-coupled damping coefficients (FT/L)
$\overline{C}$	Normalized direct damping coefficient (T)
Cr	Radial clearance; illustrated in figure 1, (L)
D	Rotor diameter (L)
K, k	Direct and cross-coupled stiffness coefficients (F/L)
$\overline{K}, \overline{k}$	Nondimensional direct and cross-coupled stiffness coefficients (dimensionless)
$f = k/C\omega$	Whirl frequency ratio (dimensionless)
L	Axial seal length (L)
P	Seal pressure (bar)
Pra	Pressure ratio = discharge pressure/supply pressure
Rs	Seal radius (L)
V	Seal inlet tangential velocity (L/T)
X, Y	Rotor to stator relative displacement components
$\dot{m}$	Seal mass flow rate (M/T)
$u_{\theta 0} = U_{\theta 0}/Rs\omega$	Nondimensional inlet tangential velocity
$U_{\theta 0}$	Inlet tangential velocity (L/T)
ω	Shaft angular velocity $(1/T)$

Subscripts

b	Sump Value
r	Reservoir value, radial component
t	Tangential component
X, Y	Rectangular coordinate directions

INTRODUCTION

Background and Motivation

One of the early steps in eliminating subsynchronous vibration problems in the Space Shuttle Main Engine(SSME) High Pressure Oxygen Turbopump(HPOTP) involved redesign of the turbine interstage seal. The redesign (Scharrer, 1989) consisted of the following sequential steps: (a) replace the original, stepped, tooth-on-rotor labyrinth with a smooth-rotor/honeycomb-stator design, and (b) introduce a swirlbrake upstream of the honeycomb seal. The initial redesign markedly reduced, but did not eliminate, the subsynchronous whirl; however, the addition of the swirl brake completely eliminated the subsynchronous motion over the full, steady-state, range of the unit.

A side view of the current seal with its installed swirlbrake is illustrated in figure 1. A detailed view of this swirl brake is provided in figure 2. A proposed alternative design is illustrated in figure 3. The current design uses radial slots to reduce the tangential velocity of the flow approaching the seal, the alternate design uses a standard aerodynamic design based on the approach velocity vector to smoothly eliminate the tangential velocity component. The alternate design turning vanes have a constant thickness and their entrance sections are not rounded. The second author of this paper developed the basic design of figure 3.

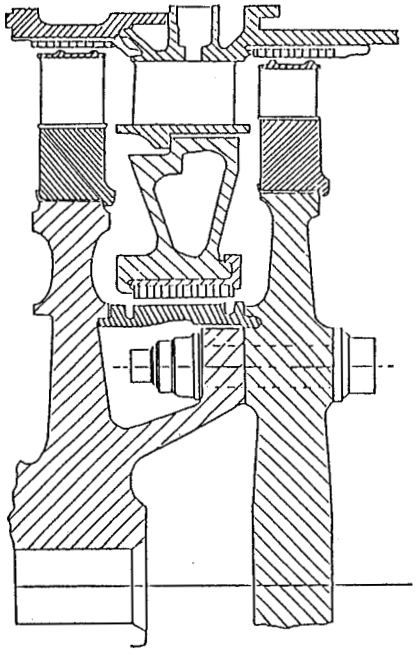

1. HPOTP turbine interstage seal(relative seal dimensions are not to scale).

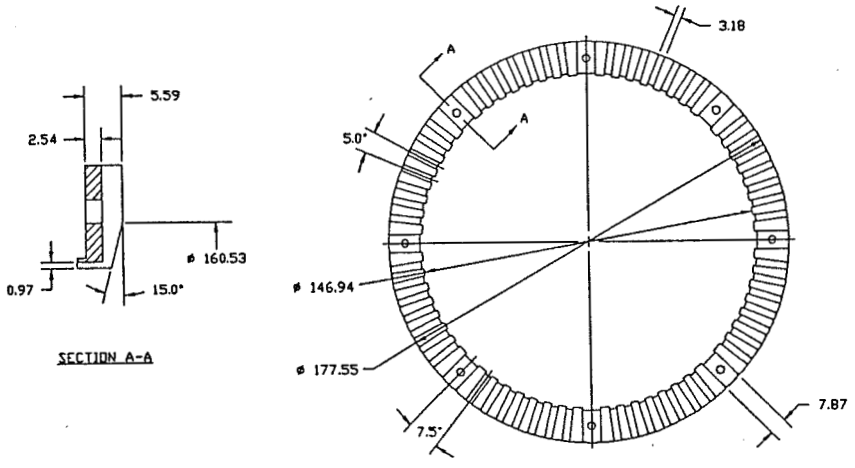

2. Current swirl-brake design.

To appreciate the design constraints on these swirl brakes, observe in figure 1 that the leakage flow approaches the seal with a predominantly radial inflow direction with very little axial velocity. The swirl brake reduces the tangential velocity or "swirl" of the leakage flow before it enters the seal to reduce the seal's rotordynamic destabilizing forces. The slots in the swirl brakes are specifically provided for this purpose. The effectiveness of the swirl brake is maximized by minimizing the axial distance between the swirl brake and the adjacent turbine wheel. Unfortunately, the large axial excursions permitted by the HPOTP balance piston at startup and shutdown force the axial spacing to higher than desirable values. The alternate design of figure 3 maintains the same(minimum) axial clearance throughout its radial expanse.

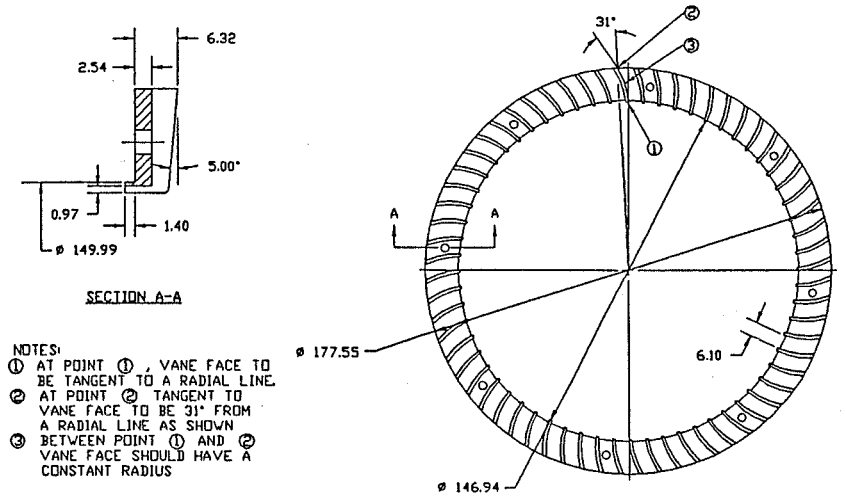

3. Alternate swirl-brake design.

Figure 4 illustrates the basic honeycomb-stator design. As illustrated, the honeycomb uses a $1.40mm$ $(0.055in)$ cell width and $3.81mm$ $(0.150in)$ cell depth. The swirl brakes are attached by screws to this piece. The seal section illustrated in figure 4 was provided by Rocketdyne; the two swirl brakes were manufactured by local machine shops.

For small motion about a centered position, the motion/reaction-force model for an annular seal is

$$-\begin{Bmatrix} R_X \\ R_Y \end{Bmatrix} = \begin{bmatrix} K & k \\ -k & K \end{bmatrix} \begin{Bmatrix} X \\ Y \end{Bmatrix} + \begin{bmatrix} C & c \\ -c & C \end{bmatrix} \begin{Bmatrix} \dot{X} \\ \dot{Y} \end{Bmatrix} \tag{1}$$

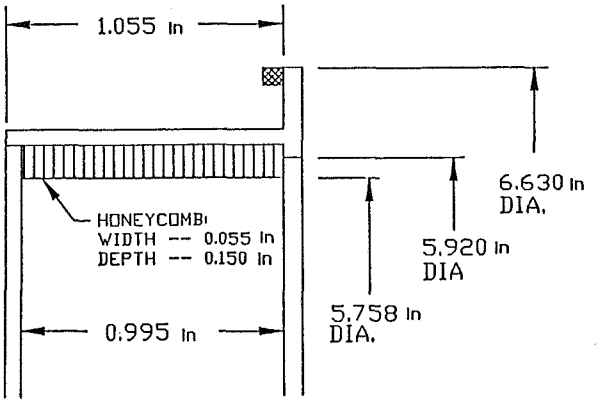

4. Seal stator dimensions.

where X,Y are components of the rotor displacement vector relative to the housing, and R_X,R_Y are components of the reaction vector acting on the rotor. Test results were obtained for the rotordynamic coefficients (K, k, C) and leakage for the HPOTP turbine interstage seal with the current and alternate swirl brakes. In terms of equation(1), swirl brakes are provided to minimize the cross-coupled stiffness coefficient k. The original published results for swirl brakes were by Benchert and Wachter(1980).

Test Apparatus Modifications

The basic configuration of the test apparatus has been discussed in several earlier publications (Childs et al., 1986, Childs and Scharrer, 1988, etc.). However, since these publications, the apparatus and facility have been modified by adding a new compressor with a consequent increase in supply pressure from 7.1 to 18 *bars*. This increase in supply pressure yields an increase in the transient forces which the rig measures. With the original compressor, the full supply pressure had to be dropped to atmosphere across the seal to achieve reasonable force amplitudes. The new compressor introduced the possibility of independently varying the back pressure (and hence pressure ratio and density) of the seal for a range of inlet pressures. Figure 5 illustrates the modifications which permit pressure-ratio control. A labyrinth back-pressure seal has been inserted downstream of the test seal. Two ports have been introduced between the test seal and the back-pressure seal for either injecting or venting air flow.

Figure 5 also illustrates a modification to the inlet flow field of the seal. In the previous apparatus, swirl vanes to prerotate the fluid were positioned immediately upstream of the seal inlet. The guide vane designs of Childs et al.(1986) were used here. The suggestion was made that introducing an axial spacing between the

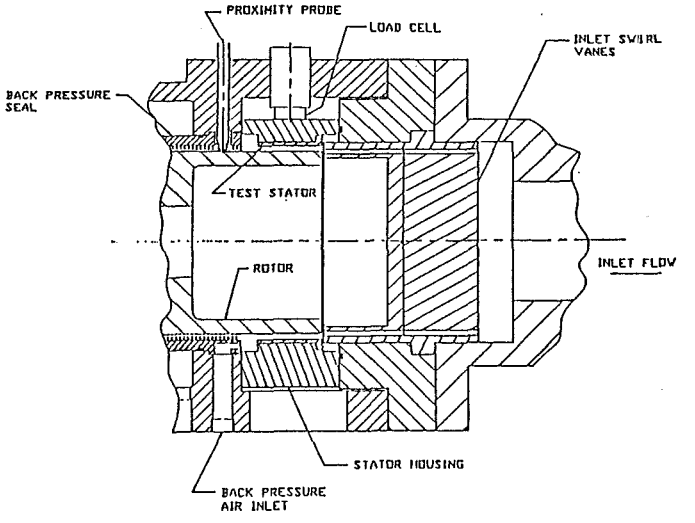

5. Back pressure and inlet modifications.

preswirl vanes and the seal could reduce "jetting" of flow from the vanes into the test seal. While the new arrangement permits direct access for measurement of the inlet velocity direction with a pitot-head probe, the velocity head is too low for accurate measurement.

Figure 6 illustrates the apparatus modification which was developed to simulate the radial approach velocity that occurs in the HPOTP. As illustrated, the preswirled flow approaches the rotor axially, proceeds radially outwards at the end of the rotor, and then radially inwards between the swirl brake and the rotor. With this design, the tangential velocity of the flow leaving the inlet guide vanes is known, but the tangential velocity of the flow actually entering the swirl brakes and the seal itself is not. The inlet preswirl arrangement illustrated in figure 6 is less than ideal, but the constraints involved in fitting the swirl brake designs into an existing apparatus precluded the development of a more representative geometry. Observe in figure 6 the axial-clearance differences for the two swirl brake designs.

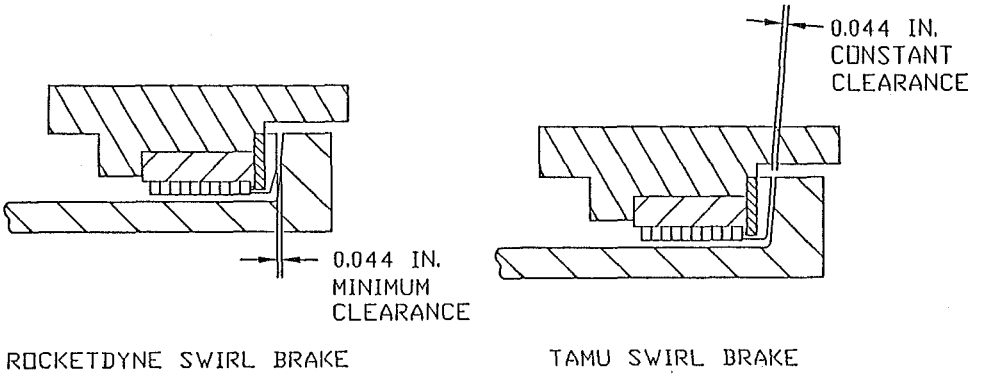

6. HPOTP turbine-interstage-seal test configuration.

Test Procedure and Parameter - Identification Changes

In addition to the above-cited changes in hardware, changes have been introduced in the excitation and parameter-identification methods. In prior tests, three different excitation frequencies were used with rotordynamic coefficients calculated at each frequency. Theoretically, the rotordynamic coefficients should be independent of excitation frequency, and the results at different excitation frequencies should be the same. For some seals, generally those with low magnitude rotordynamic coefficients, rotordynamic coefficients showed frequency dependency, while for others the coefficients were, as predicted, independent of frequency.

For the present test cases, a fast swept-sine wave excitation was used with the frequency increasing from 35 to 75 Hz. Bolleter et al.(1985) used this approach earlier for impeller tests. The excitation amplitude is around $.090mm$ with each sweep lasting approximately one second. Swept-sine-wave excitation is repeatedly applied to the rotor with intervening periods of zero-excitation of approximately 2 to 3 seconds. The no-excitation interval is inserted to allow the vibration which has been applied to the rotor to decay and to complete computer calculations. The excitation is initiated based on a phasor hole on the shaft. Hence, within reason, each swept-sine-wave excitation input and response should be identical, and by averaging the time histories of the input and response over many tests, spurious or random excitation should be reduced or eliminated. Ewins(1986) provides a thorough discussion of swept-sine-wave excitation for modal identification in conventional structural-dynamics.

To appreciate the application of swept-sine-wave excitation to the current modal identification problem, consider the following statement of the equations of motion for the seal housing.

$$M_S \begin{Bmatrix} \ddot{X}_S \\ \ddot{Y}_S \end{Bmatrix} = \begin{Bmatrix} F_{RX} \\ F_{RY} \end{Bmatrix} - \begin{bmatrix} K & k \\ -k & K \end{bmatrix} \begin{Bmatrix} X \\ Y \end{Bmatrix} - \begin{bmatrix} C & c \\ -c & C \end{bmatrix} \begin{Bmatrix} \dot{X} \\ \dot{Y} \end{Bmatrix} \tag{2}$$

F_{RX}, F_{RY} are the measured reaction forces acting on the stator housing. The acceleration components of the housing are denoted by $\ddot{X}_S, \ddot{Y}_S$ and are also measured. The test apparatus only permits motion in the X direction, hence the model becomes

$$\begin{Bmatrix} F_{RX} - M_S \ddot{X}_S \\ F_{RY} - M_S \ddot{Y}_S \end{Bmatrix} = \begin{Bmatrix} F_X \\ F_Y \end{Bmatrix} = \begin{Bmatrix} K \\ -k \end{Bmatrix} X + \begin{Bmatrix} C \\ -c \end{Bmatrix} \dot{X} \tag{3}$$

The displacement $X(t)$ is also measured and can be considered the input to the model. An analog circuit is used to generate $F_{RX} - M_S \ddot{X}_S$ and $F_{RY} - M_S \ddot{Y}_S$ from measured reaction-force and acceleration components. The swept-sine-wave excitation yields time-averaged histories $\tilde{F}_X(t_i), \tilde{F}_Y(t_i), \tilde{X}(t_i)$; $t_i = 1, 2, \ldots$ over 35 swept-sine-wave excitation inputs. The Fourier transform version of Eq. (3) is

$$\begin{Bmatrix} \hat{F}_X \\ \hat{F}_Y \end{Bmatrix} = \begin{Bmatrix} K + jC\omega \\ -k - jc\omega \end{Bmatrix} \hat{X} = \begin{Bmatrix} Z \\ -z \end{Bmatrix} \hat{X} \tag{4}$$

where the "hat" denotes Fourier-transformed variables. The variables $\hat{F}_X, \hat{F}_Y, \hat{X}$ are obtained by calculating the FFT of the time-averaged histories $\tilde{F}_X(t_i), \tilde{F}_Y(t_i), \tilde{X}(t_i)$.

The impedance functions of Eq. (4) are defined from the Fourier variables by

$$Z = \hat{F}_X/\hat{X}\,,\; z = -\hat{F}_Y/\hat{X},$$

and the rotordynamic coefficients are accordingly defined by

$$K = Re(Z)\,,\; C = Im(Z)/\omega \tag{5.a}$$

$$k = Re(z)\,,\; c = Im(z)/\omega \tag{5.b}$$

Example plots are shown in figures 7 through 9. Only frequency data from 40 to 70 Hz are used from these transfer functions in calculating rotordynamic coefficients. The average (over frequency) of $Re(\hat{F}_X/\hat{X})$ and $Re(-\hat{F}_Y/\hat{X})$ define K and k. The average slopes of $Im(\hat{F}_X/\hat{X})$ and $Im(-\hat{F}_Y/\hat{X})$ define C and c. Note in figures 7 through 9 that there is a significant deviation about the average and slopes; however, no systematic error is apparent. By a least-squares curve fit, figures 7 through 9 yield the following coefficients.

$$K = 5.46 \times 10^5 N/m,\; C = 194.0 Nsec/m$$

$$k = 2.50 \times 10^4 N/m$$

The standard deviation for these variables is

$$\sigma_K = 4.10 \times 10^3 N/m,\; \sigma_C = 8.75 Nsec/m$$

$$\sigma_k = 5.25 N/m$$

No results are presented for the cross-coupled stiffness coefficient c, because the relative uncertainty of this parameter is too high.

A review of figures 7 through 9 shows that calculation of rotordynamic coefficients at three arbitrary frequencies could yield different and quite misleading results. The swept-sine-wave approach eliminates random errors involved in the calculations and provides a basis for examination of any systematic errors due to changes in excitation frequency.

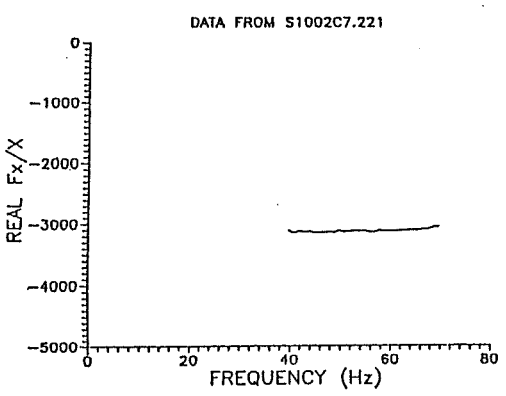

7. $Re(\hat{F}_X/\hat{X}) = K$

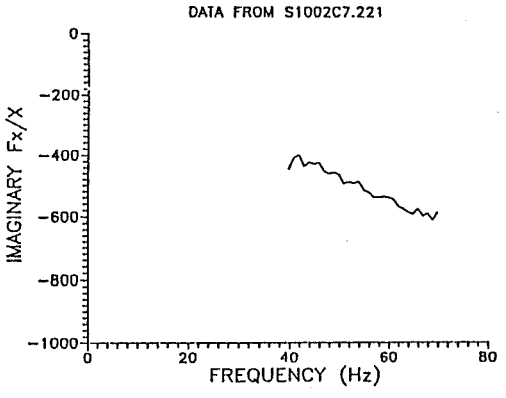

8. $Im(\hat{F}_X/\hat{X}) = C\omega$

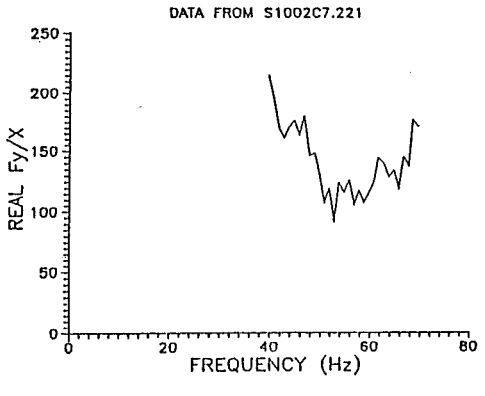

9. $Re(-\hat{F}_Y/\hat{X}) = k$

EXPERIMENTAL RESULTS

Introduction

The test apparatus and facility used for this study were developed as part of an extended, joint, NASA-USAF funded research program for annular gas seal studies. The test fluid is air. As noted in the proceeding section, the test apparatus provides an excitation about the centered position and has been thoroughly discussed in earlier publications.

Test Variables

When shaking about the centered position, the following four independent variables can be controlled: *supply pressure*, *pressure ratio*, *rotor speed*, and *inlet circumferential velocity*. The pressure ratio used here is discharge pressure divided by supply pressure; hence $Pra = 1$ implies no pressure difference, and $Pra \cong 0$ implies an infinite supply pressure. Test points for these independent variables are shown in table 1. Reference to the symbols of table 1 is helpful and necessary to understand the figures which follow.

The reservoir pressures, as measured upstream of the flowmeter, are given in table 1. These values differ (slightly) from the actual inlet pressure because of frictional losses and acceleration of the fluid due to inlet guide vanes. Tests are not run at zero pressure difference, since a small pressure difference is necessary to keep the rotor from shifting axially and rubbing the inlet-guide-vane assembly. No zero-rotor-speed tests were run, since rotor rotation is necessary to prevent damage to the thrust bearing during shaking.

Table 1. Definition of symbols used in figures.

Supply Pressures	Pressure Ratios	Rotor Speeds	Inlet Circumferential Velocities
1 - 7.9 bar 2 - 13.1 bar 3 - 18.3 bar	1 - .50 2 - .42 3 - .35 4 - .30	1 - 5000 cpm 2 - 12000 cpm 3 - 16000 cpm	0 - Zero tangential velocity 1 - Intermediate velocity with rotation 2 - High velocity with rotation

There were three test points for inlet circumferential velocity: one zero prerotation and two prerotated in the direction of shaft rotation. The zero-prerotation case is obtained with straightening vanes. The two different magnitudes of positive inlet circumferential velocity correspond to different inlet-guide-vane geometry depths. The calculated inlet tangential velocity tends to decrease with rotor speed, since the rotor grows with increased speed and reduces the leakage. The ratio of inlet circumferential velocity to rotor surface velocity ranges from zero to about 0.8.

Measurement of leakage flowrates showed no differences between the two swirl-brake designs.

Whirl-Frequency Ratio Definition

For a circular orbit of amplitude A and precessional-frequency ω, the resultant radial and tangential forces developed by the seal model of equation (1) are

$$-F_r/A = K + c\omega$$

$$F_t/A = k - C\omega \tag{6}$$

From a stability standpoint, the destabilizing tangential force F_t is of most interest. A positive cross-coupled stiffness k is destabilizing because it "drives" the forward

orbital motion of the rotor. Positive direct damping C and a negative cross-coupled stiffness are stabilizing because they oppose the orbital motion.

A convenient measure of seal stability is the whirl frequency ratio, which is a nondimensionalized ratio of cross-coupled stiffness to direct damping forces with a circular orbit.

$$whirl - frequency\,ratio = f = \frac{k}{C\omega} \tag{7}$$

Relative Uncertainty

The uncertainty in the dynamic coefficients can be determined using the method described by Holman(1978). The uncertainty in the force, excitation frequency, and displacement measurements are 0.55 N (0.125 lb), 0.065 Hz, and 0.0013 mm (0.05 mils), respectively. Before normalization, the nominal calculated uncertainty in the stiffness coefficients is 6.7 N/mm (38 lb/in) and 0.014 N-s/mm (0.082 lb-s/in) for the damping coefficients. The predicted uncertainties are generally satisfactory in comparison to nominal values for K, k, and C.

The principal source of uncertainty in the *resultant* force measurement is the acceleration measurement for the stator, not the piezo-electric force transducer measurements. The "normal" accelerometers used in the tester have a resolution of 5 x 10^{-3} g's. Although more sensitive accelerometers are available, they can not generally be used when testing honeycomb seals, because high-frequency accelerometer "spikes" are frequently seen with these seals, presumably because of a Helmholtz-acoustic excitation.

Test Results

Figure 10 illustrates K for the current(Rocketdyne) swirl brake design versus inlet tangential velocity for three supply pressures and four pressure ratios. Generally speaking, K increases with increasing running speed, supply pressure, and pressure ratio. Although not illustrated, comparable results are obtained with the alternate(TAMU) swirl brake design. The increase in K with increasing running speed arises due to a reduction in clearance. When K is nondimensionalized, removing the influence of clearance changes, no speed influence is present.

Figure 11 illustrates k for the current and alternate swirl brake designs. Observe that the alternate swirl-brake design consistently yields much lower values for this coefficient. In some cases, the alternate design actually yields negative values for k versus positive values for the current design. Negative k values would oppose forward whirl of the turbopump.

Figure 12 illustrates C for the current swirl brake. C is observed to decrease slightly with increasing running speed. Although not illustrated, comparable damping results were obtained for the alternate swirl brake design.

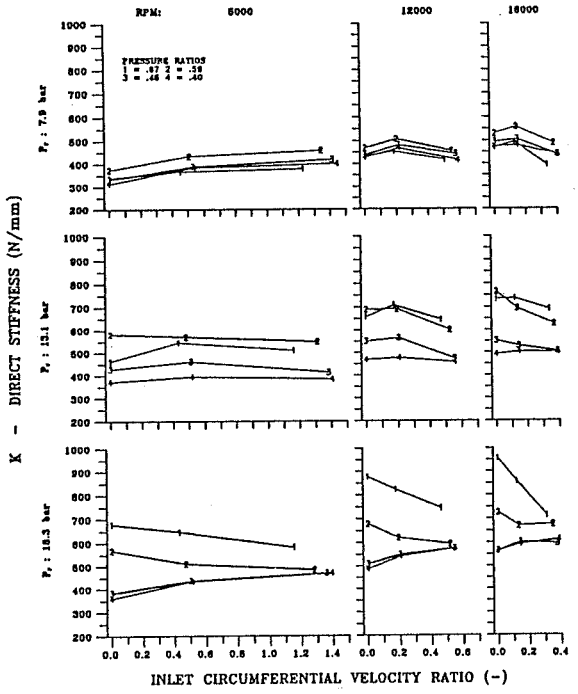

10. Direct stiffness K for the current swirl-brake design.

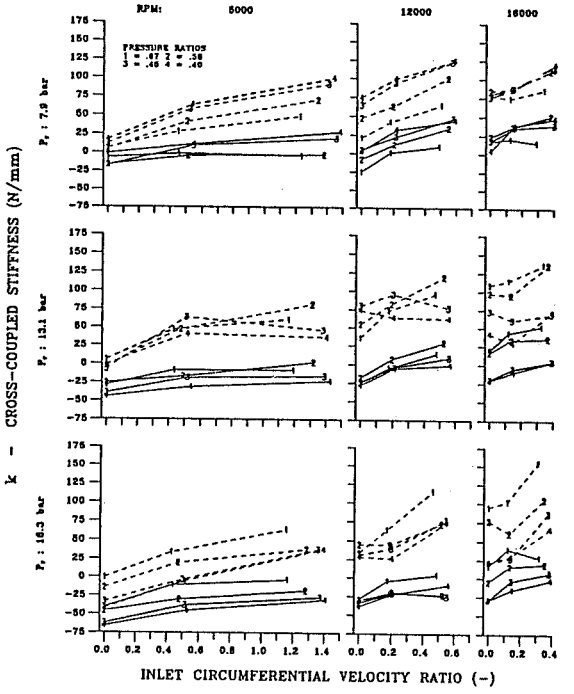

11. Cross-coupled-stiffness k for the current and alternate swirl-brake designs.

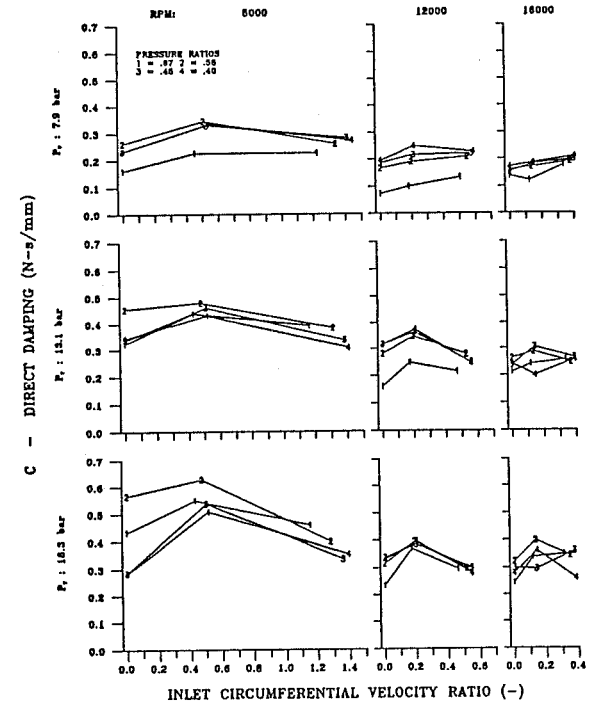

12. Direct damping C for the current swirl-brake design.

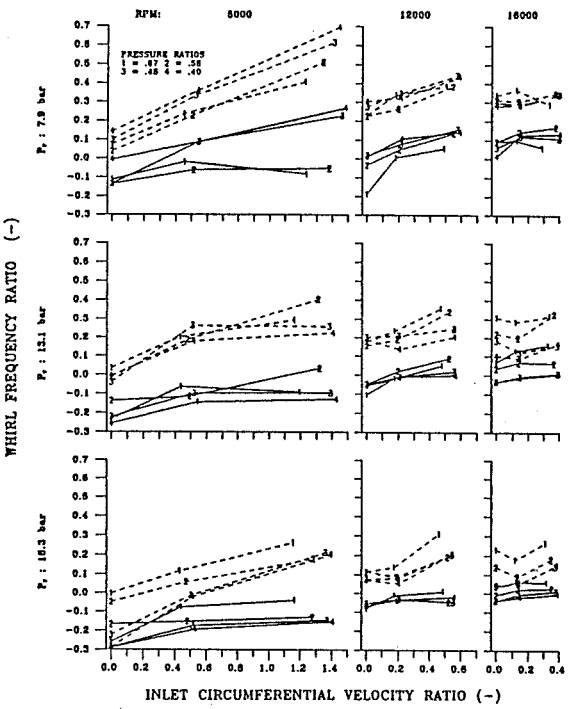

13. Whirl-frequency ratio f for the current and alternate swirl-brake designs.

Figure 12 illustrates C for the current swirl brake. C is observed to decrease slightly with increasing running speed. Although not illustrated, comparable damping results were obtained for the alternate swirl brake design.

Figure 13 illustrates the whirl-frequency ratio f for the current and alternate swirl-brake designs demonstrating the improved rotordynamic-stability performance of the alternate design. In all cases, the alternate design yields lower values for f. In many cases, the alternate design yields negative values for f versus positive values for the current design.

As noted in the introduction, the present tests include the pressure ratio as a parameter for the first time. Field experiences have demonstrated that centrifugal compressors using teeth-on-stator labyrinth seals become less stable as the average density is increased, Kirk and Donald(1983). One of the influences of a change in pressure ratio with a fixed supply pressure is a density variation of the fluid within the seal. Specifically, as the pressure ratio is increased, the density increases while ΔP decreases. From figure 13, at the lowest speed and supply pressure, stability is improved by increasing the pressure ratio(and average density) and decreasing ΔP. However, at the highest supply pressure, stability is improved by decreasing the pressure ratio, i.e., decreasing density while increasing ΔP. The high supply-pressure results are consistent with Kirk and Donald's experience with centrifugal compressors.

SUMMARY AND CONCLUSIONS

Test results are presented for the rotordynamic coefficients of the HPOTP turbine interstage seal with the current swirl brake and an alternate design swirl brake. The two swirl-brake designs yield identical leakage performance and comparable results for direct stiffness and damping; however, the alternate design has much better stability performance over all operating conditions.

Test results since Benchert and Wachter(1980) demonstrate that almost any swirl brake will improve rotordynamic stability by reducing the inlet tangential velocity and consequently reducing the cross-coupled stiffness coefficient. However, the stability improvement accruing to an aerodynamic design is clearly demonstrated to be substantial by the present test results. Given the critical nature of these devices for rotordynamic stability of many machines, a thorough aerodynamic design is clearly in order.

REFERENCES

Benchert, H., and Wachter, J.(1980), "Flow Induced Spring Coefficients of Labyrinth Seals for Application in Rotordynamics," NASA CP2133, Proceedings of the workshop: Rotordynamic Instability Problems in High Performance Turbomachinery, held at Texas A&M University, 12-14 May 1980, pp. 189-212.

Bolleter, U., Wyss, A., Welte, I., and R. Sturchler, (1985), "Measurement of Hydrodynamic Matrices of Boiler Feed Pump Impellers," *ASME Journal of Vibrations, Stress and Reliability in Design,* Vol. 109, pp. 144-151.

Childs, D. W., and Scharrer, J.(1988), "Theory Versus Experiment for the Rotordynamic Coefficients of Labyrinth Gas Seals: Part II - A Comparison to Experiment," *ASME Journal of Vibration, Acoustics, Stress, and Reliability in Design,* Vol. 110, No. 3, July 1988, pp. 281-287.

Childs, D. W., Nelson, C. E., Nicks, C., Scharrer, J., Elrod, D., and Hale, K.(1986), "Theory Versus Experiment for the Rotordynamic Coefficients of Annular Gas Seals: Part 1-Test Facility and Apparatus",*ASME Transaction Journal of Tribology,* Vol. 108, pp. 426-432.

Ewins, D. J.(1986), "Modal Testing: Theory and Practice," Research Studies Press Ltd.

Kirk, R. G., and Donald, G. N.(1983), "Design Criteria for Improved Stability of Centrifugal Compressors," Rotor Dynamical Instability, ASME presented at *The Applied Mechanics, Bioengineering and Fluids Engineering Conference,* Houston, Texas, 20-22 June 1983.

Holman, J. P.(1978), *Experimental Methods for Engineers,* McGraw Hill, 1978, pp. 45.

Scharrer, J.(1989), discussion of the paper, "Annular Honeycomb Seals: Test Results for Leakage and Rotordynamic Coefficients; Comparisons to Labyrinth and Smooth Configurations," by D. Childs et al., *ASME Journal of Tribology,* pp. 793-301.